Mixed Grid-Forming and Grid-Following Inverters with Secondary Control Providing Fast Voltage and Frequency Support

Huang, Liang; Wu, Chao; Zhou, Dao; Blaabjerg, Frede

Published in:
Proceedings of the 2023 25th European Conference on Power Electronics and Applications (EPE'23 ECCE Europe)

DOI (link to publication from Publisher):
10.23919/EPE23ECCEEurope58414.2023.10264435

Publication date:
2023

Document Version
Accepted author manuscript, peer reviewed version

Mixed Grid-Forming and Grid-Following Inverters with Secondary Control Providing Fast Voltage and Frequency Support

Liang Huang[1], Chao Wu[2], Dao Zhou[1], and Frede Blaabjerg[1]
[1]AAU Energy, Aalborg University
Pontoppidanstræde 101, 9220 Aalborg East, Aalborg, Denmark
[2]Department of Electrical Engineering, Shanghai Jiao Tong University
Dongchuan Road 800, Shanghai, China
E-Mail: lihu@energy.aau.dk, wuchao@sjtu.edu.cn, zda@energy.aau.dk, fbl@energy.aau.dk
URL: https://www.energy.aau.dk/

Keywords

«Grid-connected inverter», «Grid forming», «Reactive power», «Voltage regulation», «Stability».

Abstract

As the penetration of renewable energy generation increases, grid-forming (GFM) inverters are deemed to be a promising solution for future power systems. However, restricted by the power rating of the inverter, the limited power output ability makes GFM inverters behave not exactly the same as synchronous generators. Namely, GFM inverters may have difficulties in meeting all the Grid Codes simultaneously. When the active power requirement is prioritized to be satisfied by GFM inverters, the reactive power requirement may be difficult to meet at the same time. To address this issue, a mixed GFM and grid-following inverter scheme is proposed, where the GFM inverter is prioritized to provide active power to support the grid frequency while the GFL inverter is prioritized to provide reactive power to support the grid voltage. It is found that the proposed mixed scheme can provide fast voltage and frequency support in weak grid case.

Introduction

Due to economic, energy, and environmental issues, the fossil-fuel-based energy source is considered to be unsustainable and unclean. So, installing renewable energy sources (e.g., wind power and solar power) have been grown rapidly in recent years [1]. However, as the penetration of renewable generation increases, conventional synchronous generators will be replaced by inverter-based resources (IBRs) gradually [2]. Consequently, the total inertia of the power system and the grid strength will be decreased. Thus, the power grid will become weaker and may lead to voltage and frequency instability issues [3].

To ensure that the power system operates safely, stably, and economically, the grid voltage magnitude at each bus is required to be controlled within ±5% ~ ±10% of the nominal voltage. Besides, the grid frequency of the power system is required to be regulated within ±0.5 Hz around the nominal frequency (i.e., 50 Hz or 60 Hz) in the normal situation [4]. However, as the power grid becomes weaker, voltage and frequency stability requirements are difficult to be maintained [5]. Specifically, for the low-inertia grid, remaining the frequency stability is a challenge, while the voltage stability is hard to be kept in a low short-circuit ratio (SCR) grid [6]–[10]. In addition, the conventional grid-connected inverters with grid-following (GFL) control behave like a current source, which relies on an external voltage source for normal operation. Thus, GFL inverters are difficult to operate in the islanded case [11]. With this background, grid-connected inverters with grid-forming (GFM) control have attracted more attention in recent years [12]–[14]. Different from GFL inverters, GFM inverters behave like a voltage source, so they can operate in islanded conditions as well as provide frequency support to assist in keeping the frequency stability [15]. Thus, the frequency stability issues can be addressed easily by using GFM inverters [16]–[18].

In order to make GFM inverters keep a stronger voltage source characteristic, the reactive power tracking speed is usually designed to be slow [19]. Otherwise, the stability of GFM inverters might be jeopardized. However, although a slow reactive power control is beneficial for stability, it limits the voltage support capability in weak

grid cases. Thus, grid-connected inverters with pure GFM control may have limited voltage support ability in weak grid cases. Besides, when the output current is limited within the maximum value (typically 1 ~ 1.2 p.u.), GFM inverters may take too much burden to provide both frequency support and voltage support simultaneously, because when the requirement of the active power is satisfied preferentially, the requirement of the reactive power is difficult to be fulfilled at the same time. Hence, grid-connected inverters with pure GFM control may not be an optimal solution in terms of voltage support ability in weak grids.

Based on previous study experience, it is known that GFL inverters can track the reactive power reference quickly to provide voltage support [20], which is beneficial to maintain the voltage stability of the system. Considering a mixed GFM and GFL inverter scheme may have complementary benefits [21], this paper provides a comparative study of paralleled grid-connected inverters with pure GFM control and with mixed GFM plus GFL controls. The study results show that the mixed GFM and GFL inverters have better performance than pure GFM inverters (i.e., faster voltage support and frequency support in both strong and weak grid cases).

Configuration of case study system

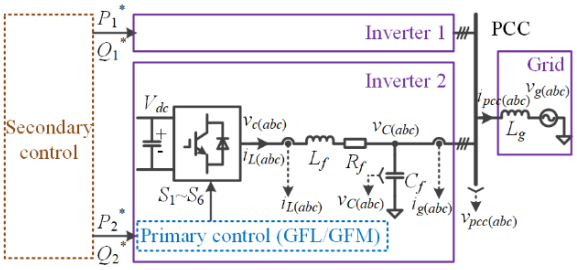

Fig. 1: Study case of two paralleled inverters connected to Thevenin equivalent grid.

The proposed case study system is shown in Fig. 1, which includes two inverters connected to a Thevenin equivalent grid at the point of common coupling (PCC). On the grid side, L_g represents the grid inductance, and $v_{g(abc)}$ represents the three-phase grid voltage. On the inverter-side, two inverters are connected in parallel. Considering that Inverter 1 and Inverter 2 are completely the same, only the internal structure of Inverter 2 is presented in Fig. 1. It can be seen from Fig. 1 that the inverter system includes a dc voltage source, a three-phase inverter, and L-C filters. Each inverter is controlled by a primary control scheme, which could be GFL or GFM control. Besides, the power reference of each inverter comes from the secondary control. The detailed control schemes will be introduced as follows.

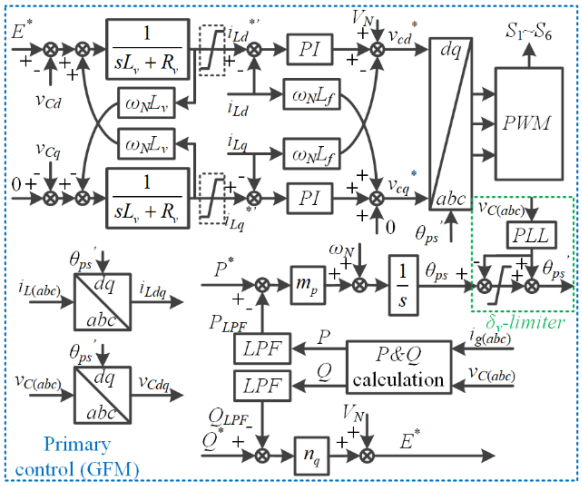

Fig. 2: Grid-forming-based primary control scheme.

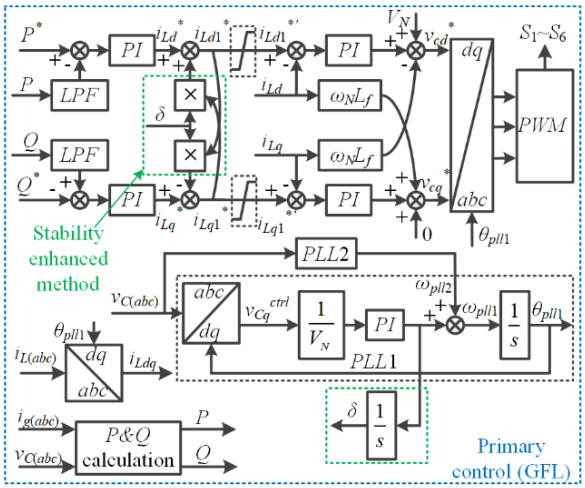

Fig. 3: Grid-following-based primary control scheme.

As aforementioned, for each inverter, the primary control can be achieved by either the GFL or GFM control. Fig. 2 shows a typical droop control-based GFM control scheme and it is selected in this paper for the case study, where the proportional-integral (PI) control is used to control the current and the virtual admittance control is used to regulate the voltage. Besides, a power angle limitation method (like that given by [22]) is applied to protect the GFM inverter against overcurrent. In addition, as shown in Fig.

3, a double-PLL-based stability-enhanced GFL control scheme (like that given by [20]) is also selected.

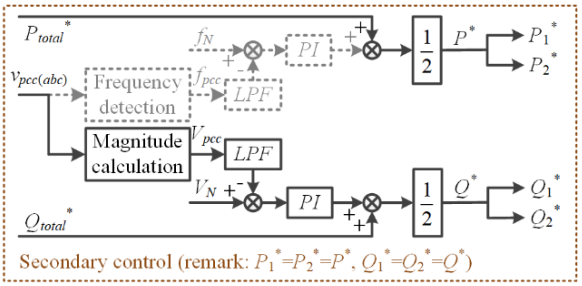

Fig. 4: Secondary control for generating active and reactive power reference.

A secondary control scheme with PCC voltage magnitude control and frequency control as shown in Fig. 4 is applied. The input power reference of the whole system is (P_{total}^*, Q_{total}^*). For the two inverters, the total output power reference is divided by two to give each inverter their reference. Notably, since the study focus is on reactive power control and voltage support, the frequency control block in Fig. 4 is disabled, but it could also be implemented.

Steady-state and dynamic analysis for GFL and GFM inverters

According to existing studies [20], [23], it is known that the small-signal stability of the selected GFL and GFM control scheme are already satisfied, because they can be stabilized within a wide range of SCRs (e.g., 1 ~ 30). Based on that, this paper will analyze their external characteristics.

A. Steady-state performance analysis

As shown in Fig. 3, for the selected GFL control scheme, both the active and reactive power are controlled by PI controllers. So, the steady-state error of the power control is zero. Thus, the steady-state active and reactive power are equal to the reference values, as presented in (1).

$$\begin{cases} P_{GFL} = P_{GFL}^* \\ Q_{GFL} = Q_{GFL}^* \end{cases} \quad (1).$$

Differently, for the selected GFM control scheme, both the active and reactive power are controlled by droop controllers, as shown in Fig. 2. Thus, the steady-state error of the power control depends on the droop coefficient. The steady-state expressions of the active and reactive power can be derived as:

$$\begin{cases} P_{GFM} = P_{GFM}^* - \frac{\omega_g - \omega_N}{m_p} \\ Q_{GFM} = Q_{GFM}^* - \frac{E^* - V_N}{n_q} \end{cases} \quad (2).$$

where steady-state value of E^* depends on grid voltage V_g, grid inductance L_g, and active power P_{GFM}.

B. Dynamic performance analysis

Moreover, to analyze the dynamic performance of GFL and GFM inverters, their closed-loop transfer functions of the power loop need to be calculated, which will be discussed as follows.

Firstly, for the GFL inverters, the PLL can lock the phase angle of the PCC voltage to make the q-axis voltage $v_{pcc,q}$ equal to zero. So, the active power and reactive power can be deduced as:

$$\begin{cases} P_{GFL} = \frac{3}{2} V_{pcc,d} \cdot i_d \\ Q_{GFL} = \frac{-3}{2} V_{pcc,d} \cdot i_q \end{cases} \quad (3).$$

Assuming the inner current control loops are much faster than the outer power control loops, the open-loop transfer functions of the power control loops can be obtained as:

$$\begin{cases} T_{ol,P,GFL} = (k_{p,P} + \frac{k_{i,P}}{s})(\frac{3}{2} V_{pcc,d}) \frac{\omega_{LPF}}{s+\omega_{LPF}} \\ T_{ol,Q,GFL} = (k_{p,Q} + \frac{k_{i,Q}}{s})(\frac{-3}{2} V_{pcc,d}) \frac{\omega_{LPF}}{s+\omega_{LPF}} \end{cases} \quad (4).$$

where $k_{p,P} = \omega_p/(1.5V_N \cdot \omega_{LPF})$, $k_{i,P} = \omega_p/(1.5V_N)$, $k_{p,Q} = \omega_q/(-1.5V_N \cdot \omega_{LPF})$, and $k_{i,Q} = \omega_q/(-1.5V_N)$.

Based on (4), the closed-loop transfer functions of the power control loops can be derived as:

$$\begin{cases} T_{cl,P,GFL} = \frac{\omega_p}{s+\omega_p} \\ T_{cl,Q,GFL} = \frac{\omega_q}{s+\omega_q} \end{cases} \quad (5).$$

Differently, for the GFM inverters, the active power and reactive power depend on the power angle and voltage magnitude, as shown in (6).

$$\begin{cases} P_{GFM} = \frac{3}{2} \frac{V_g \cdot E^* \cdot \sin(\delta)}{X_v + X_g} \approx \frac{3}{2} \frac{V_g \cdot E^* \cdot \delta}{X_v + X_g} \\ Q_{GFM} \approx \frac{3}{2} \frac{V_g \cdot [E^* \cdot \cos(\delta) - V_g]}{X_v + X_g} \approx \frac{3}{2} \frac{V_g \cdot (E^* - V_g)}{X_v + X_g} \end{cases} \quad (6).$$

where V_{pcc} is assumed to be close to V_g and δ is assumed to be smaller than 30 degrees.

Also, assuming the inner current control loops are much faster than the outer power control loops, then the open-loop transfer functions of the power control loops can be provided by:

$$\begin{cases} T_{ol,P,GFM} = m_p \cdot \frac{1}{s} \cdot \left(\frac{3}{2}\frac{V_g \cdot E^*}{X_v + X_g}\right) \frac{\omega_{LPF}}{s+\omega_{LPF}} \\ T_{ol,Q,GFM} = n_q \cdot \left(\frac{3}{2}\frac{V_g}{X_v + X_g}\right) \frac{\omega_{LPF}}{s+\omega_{LPF}} \end{cases} \quad (7).$$

where $m_p = m_{p(p.u.)} \cdot \omega_N / P_N$, and $n_q = n_{q(p.u.)} \cdot V_N / P_N$.

Based on (7), the closed-loop transfer functions of the power control loops can be derived as:

$$\begin{cases} T_{cl,P,GFM} \approx \dfrac{\frac{m_{p(p.u.)}\omega_N \omega_{LPF}}{X_{v(p.u.)} + X_{g(p.u.)}}}{s^2 + \omega_{LPF} \cdot s + \frac{m_{p(p.u.)}\omega_N \omega_{LPF}}{X_{v(p.u.)} + X_{g(p.u.)}}} \\ T_{cl,Q,GFM} \approx \dfrac{\frac{n_{q(p.u.)}\omega_{LPF}}{X_{v(p.u.)} + X_{g(p.u.)}}}{s + \omega_{LPF} + \frac{n_{q(p.u.)}\omega_{LPF}}{X_{v(p.u.)} + X_{g(p.u.)}}} \end{cases} \quad (8).$$

Case studies of two paralleled grid-connected inverters

In the previous section, the analytical closed-loop transfer functions of GFL and GFM inverters have been derived. To have more intuitive understanding of the advantages and disadvantages of the selected control schemes, this section will provide more specific numerical analysis by using the parameters of 4 MW (690 VAC phase-to-phase) GFL and GFM inverters listed in Table I as an example.

A. Case study of closed-loop transfer function of GFM inverters

Firstly, a strong grid condition with SCR = 10 (i.e., L_g = 0.1 p.u.) is considered. Substituting the parameters m_p, n_q, ω_N, ω_{LPF}, L_v and L_g into (8), the numerical expressions of the closed-loop transfer functions are given by:

$$\begin{cases} T_{cl,P,GFM} \approx \dfrac{19.8^2}{s^2 + 2 \cdot 0.76 \cdot 19.8 \cdot s + 19.8^2} \\ T_{cl,Q,GFM} \approx 0.2 \cdot \dfrac{37.5}{s+37.5} \end{cases} \quad (9).$$

It can be seen from (9) that the gain of the active power loop is 1 and the bandwidth is around 32 rad/s. Besides, the gain of the reactive power loop is 0.2 and the bandwidth is 37.5 rad/s.

Table I: Parameters of the study system

Parameters	Values
Rated active power, P_N	4 MW (1 p.u.)
Rated voltage (phase to ground, peak value), V_N	563 V (1 p.u.)
Fundamental angular frequency, ω_N	2π·50 Hz
Rated dc voltage, V_{dc}	1200 V
Filter inductance, L_f	0.15 p.u.
Filter resistance, R_f	0.005 p.u.
Filter capacitance, C_f	0.02 p.u.
GFL-based primary control scheme	
Current loop bandwidth, ω_i	4000 rad/s
PLL bandwidth, ω_{pll}	400 rad/s
Reactive power loop bandwidth, ω_q	50 rad/s
Active power loop bandwidth, ω_p	10 rad/s
LPF cut-off angular frequency, ω_{LPF}	30 rad/s
AC current limitation, I_{lim}	1 p.u.
GFM-based primary control scheme	
Current loop bandwidth, ω_i	4000 rad/s
Virtual inductance, L_v	0.5 p.u.
Virtual resistance, R_v	0.05 p.u.
P-droop coefficient, m_p	2.5%·ω_N/P_N
Q-droop coefficient, n_q	10%·V_N/P_N
LPF cut-off angular frequency, ω_{LPF}	30 rad/s
AC current limitation, I_{lim}	1 p.u.
Secondary control scheme	
Number of inverters, N	2
AC voltage magnitude control loop bandwidth, ω_{vac}	50 rad/s

Secondly, a weak grid condition with SCR = 2 (i.e., L_g = 0.5 p.u.) is considered. Substituting the parameters m_p, n_q, ω_N, ω_{LPF}, L_v and L_g into (8), the numerical expressions of the closed-loop transfer functions can be deduced as:

$$\begin{cases} T_{cl,P,GFM} \approx \dfrac{15.4^2}{s^2 + 2 \cdot 0.97 \cdot 15.4 \cdot s + 15.4^2} \\ T_{cl,Q,GFM} \approx 0.13 \cdot \dfrac{34.5}{s+34.5} \end{cases} \quad (10).$$

It can be seen from (10) that the gain of the active power loop is 1 and the bandwidth is around 25 rad/s. Besides, the gain of the reactive power loop is 0.13 and the bandwidth is 34.5 rad/s, which are smaller than the gain and bandwidth of the first case (SCR = 10).

Based on the above analysis, it is known that the output reactive power of the droop-based GFM inverters with virtual admittance has difficulties in following the reference, because its closed-loop gain is much lower than 1. Besides, as the grid inductance L_g increases, the weak grid case is worse than the strong grid case.

B. Case study of closed-loop transfer function of GFL inverters

Different from GFM inverters, the closed-loop transfer functions of GFL inverters do not depend on the grid impedance. Namely, no matter whether the grid is strong or weak, they are the same, as shown in (5). Hence, the bandwidth of the reactive power control loop can be designed relatively higher (e.g., 50 rad/s) to have better dynamic performance. When substituting the parameters ω_p and ω_q into (5), the numerical expressions of the closed-loop transfer functions can be derived as:

$$\begin{cases} T_{cl,P,GFL} = \frac{10}{s+10} \\ T_{cl,Q,GFL} = \frac{50}{s+50} \end{cases} \quad (11).$$

It can be seen from (11) that the gain of the reactive power loop is 1 and the bandwidth is 50 rad/s. Hence, the reactive power tracking performance of the GFL inverters should be superior to that of the GFM inverters.

Based on the above analysis, a mixed GFL and GFM inverter scheme should have better reactive power control performance than a pure GFM inverter scheme. Thus, the active power requirements in the Grid Code can be satisfied by GFM inverters, while the reactive power requirements in the Grid Code can be satisfied by GFL inverters in the mixed GFL and GFM inverter scheme. Simulation studies will be introduced to demonstrate that.

To verify the above analysis, two paralleled grid-connected inverters are modeled in MATLAB/Simulink, where the system configuration is the same as that shown in Fig. 1. Moreover, the control parameters are the same as that listed in Table I. The simulation results of the two grid-connected inverters in different grid strength cases are shown in Figs. 5 ~ 8, where a mixed GFM and GFL inverter scheme and a pure GFM inverter scheme are compared to see their voltage and frequency support ability.

Fig. 5 shows the simulation results of a strong grid case with SCR = 10. In the beginning, a 0.5 p.u. of power reference is given to each of the two inverters. The power step response time of GFM inverter is around 0.2 seconds (underdamped) and the response time of GFL inverter is 0.3 seconds, which agree with the theoretical analysis in the previous section. Then, at the instant of 2.1s, the grid frequency is reduced by 0.3 Hz for the two GFM inverter case, while the grid frequency is reduced by 0.6 Hz for the mixed GFM+GFL inverter case (Note: two cases support the same amount of the active power). GFM inverters provide additional active power to support the grid frequency, while the GFL inverter does not support the grid frequency. It shows that the performances of both cases are acceptable. Although GFM inverters have a slower reactive power response, it does not matter in the strong grid case, because the PCC voltage is always close to 1 p.u.

Fig. 6 shows the simulation results of a weak grid case with SCR = 2. Initially, the active power is 0.5 p.u. Then, the grid frequency is reduced by 0.3 Hz and 0.6 Hz for each case in Figs. 6(a) and (b). GFM inverters provide extra active power to support the grid frequency. Meanwhile, the reactive power reference from the secondary control is increased because the PCC voltage magnitude is lower than the nominal value. It can be seen from Fig. 6(a) that even though the reactive power reference of the two GFM inverter case is increased to 1 p.u., just a little reactive power is provided from the GFM inverter. Differently, as shown in Fig. 6(b), the GFL inverter can quickly follow the reactive power reference to support the grid voltage. Thus, the GFL inverter seems to have better voltage support performance than the GFM inverter. Even so, since the PCC voltage magnitude is close to 1 p.u., the differences between the two cases are not obvious. So, the performances of both study cases in Fig. 6 are still acceptable.

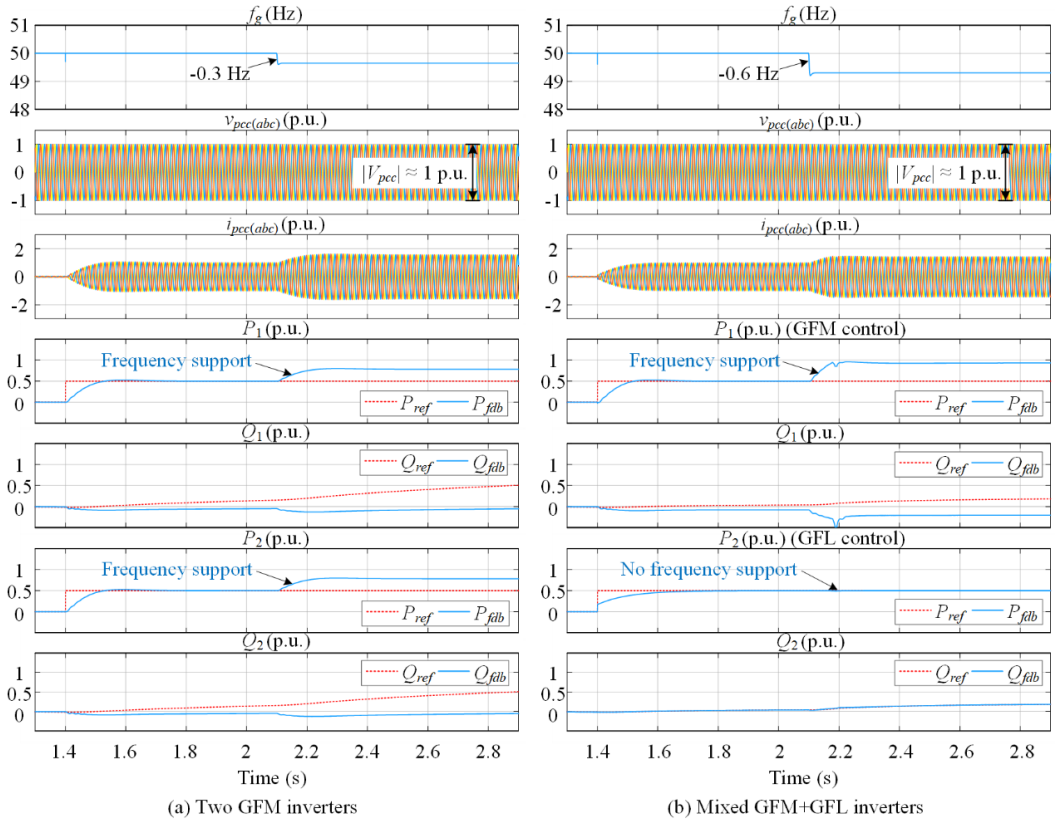

(a) Two GFM inverters (b) Mixed GFM+GFL inverters

Fig. 5: Simulation results of two paralleled inverters when the grid frequency is dropped by 0.3 or 0.6 Hz in a strong grid case (SCR = 10).

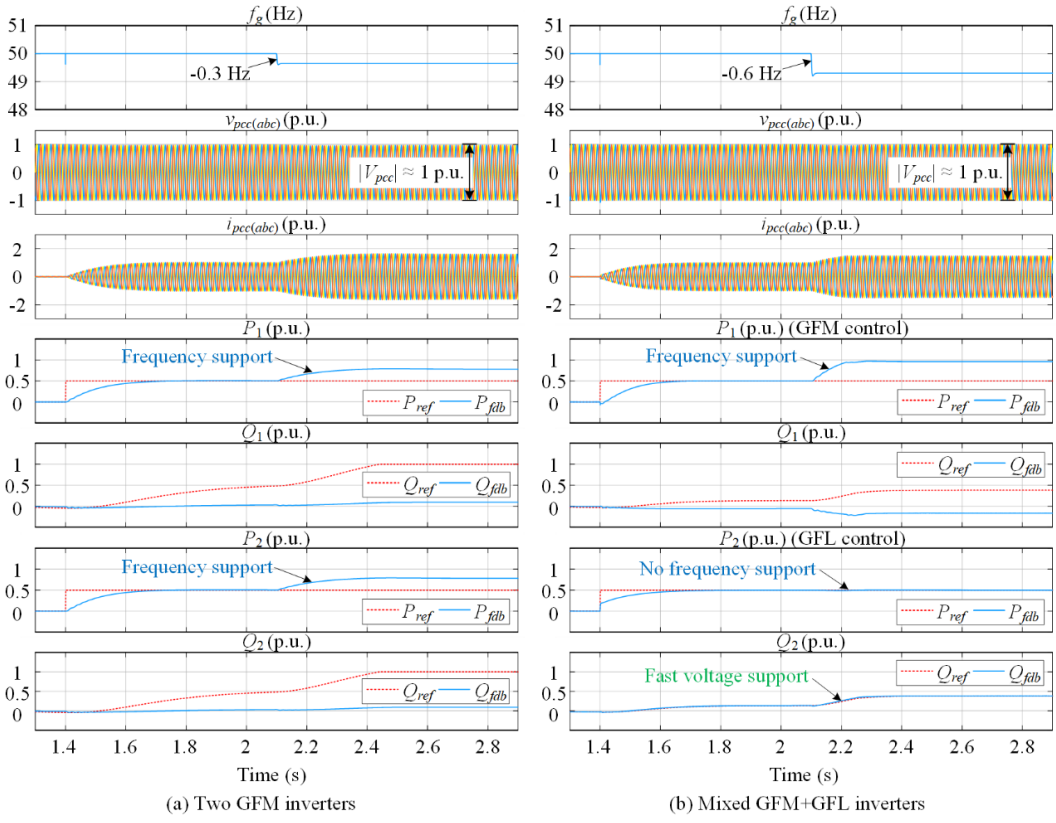

(a) Two GFM inverters (b) Mixed GFM+GFL inverters

Fig. 6: Simulation results of two paralleled inverters when the grid frequency is dropped by 0.3 or 0.6 Hz in a weak grid case (SCR = 2).

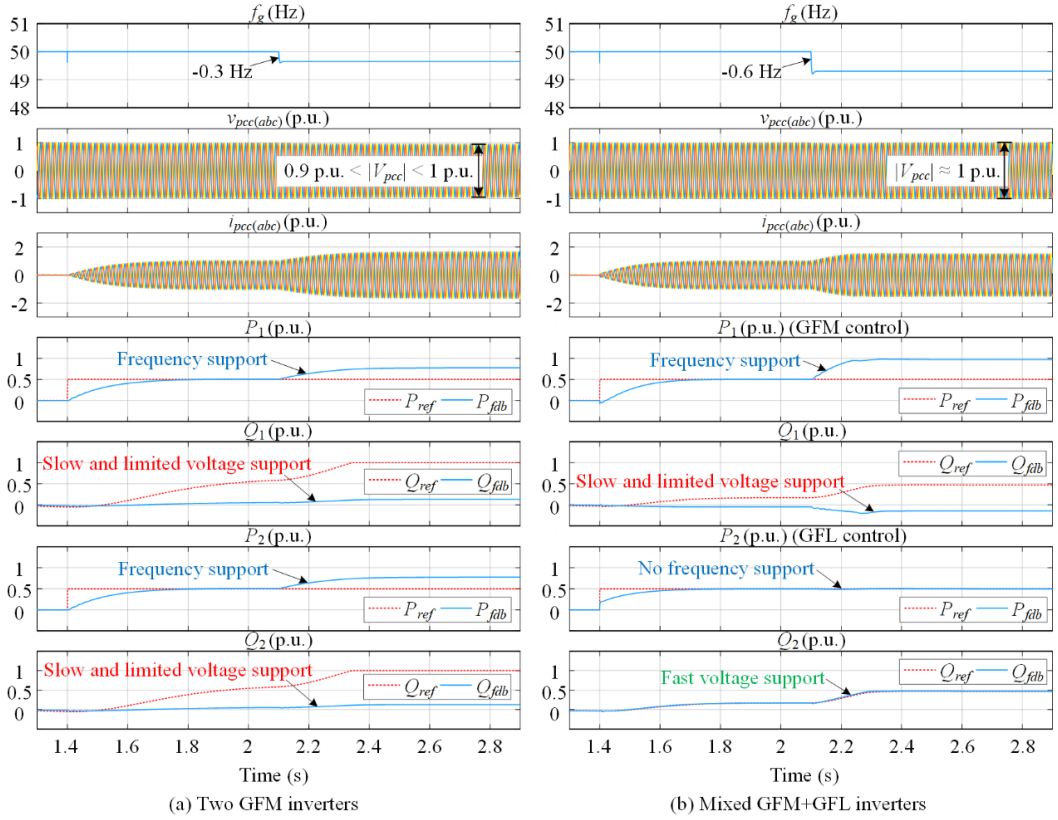

Fig. 7: Simulation results of two paralleled inverters when the grid frequency is dropped by 0.3 or 0.6 Hz in a weak grid case (SCR = 1.5).

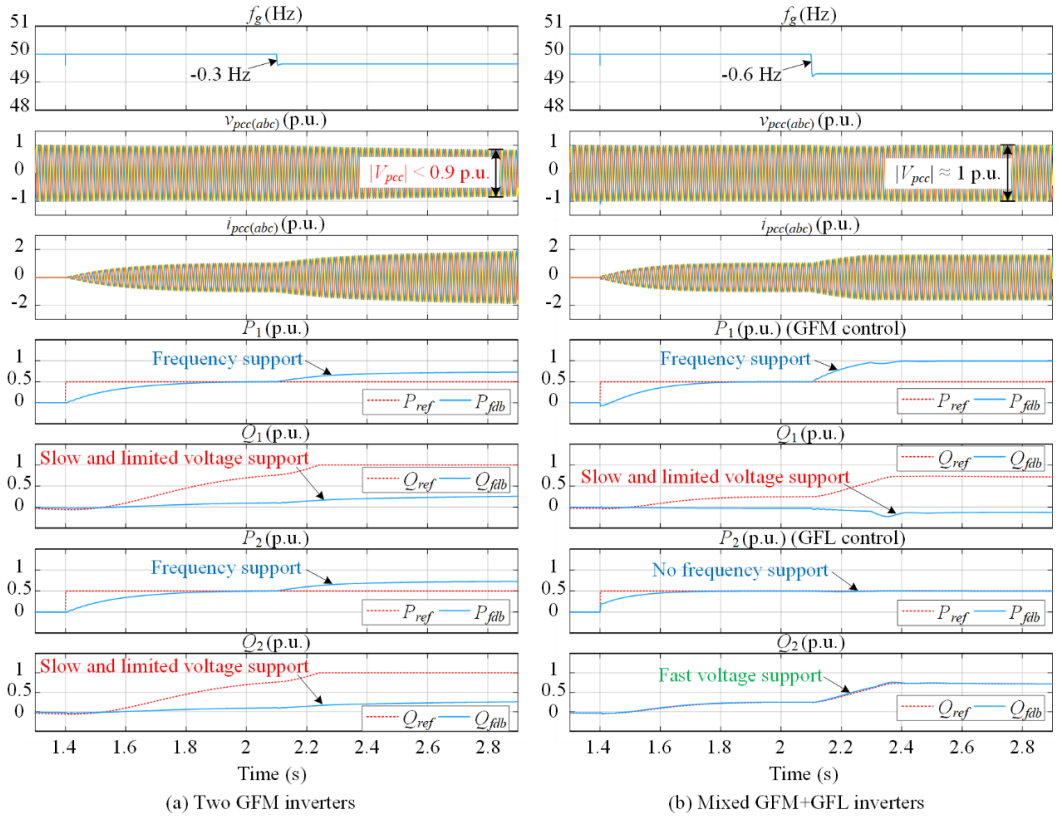

Fig. 8: Simulation results of two paralleled inverters when the grid frequency is dropped by 0.3 or 0.6 Hz in an ultra-weak grid case (SCR = 1).

Table II: Comparison of three possible cases

Cases	Frequency support	Voltage support
Pure GFL	No	Fast
Pure GFM	Fast	Slow & limited
Mixed GFL+GFM	Fast	Fast

Fig. 7 shows the simulation results of a weak grid case with SCR = 1.5 and Fig. 8 shows the simulation results of an ultra-weak grid case with SCR = 1. It can be seen from Fig. 7(a) that as the active power increases, the magnitude of the PCC voltage is reduced to be lower than 1 p.u. (but higher than 0.9 p.u.) due to limited reactive power control ability of the GFM inverters. In addition, it can be seen from Fig. 8(a) that as the active power increases, the magnitude of the PCC voltage is reduced to be lower than 0.9 p.u., which is not acceptable. Hence, the poor reactive power tracking ability might be a problem for the pure GFM inverter scheme.

However, as shown in Fig. 7(b) and Fig. 8(b), for the mixed scheme, the grid frequency can be supported by the GFM inverter, and the magnitude of the PCC voltage can be supported by the GFL inverter under weak grid conditions. So, the mixed GFL and GFM inverter scheme can improve the reactive power tracking ability of the pure GFM inverter scheme.

Notably, another case of pure GFL inverters has been studied a lot in existing research [18], so it will not be discussed in this paper. To compare the performance of frequency support and voltage support in different cases, the advantages and disadvantages of three possible cases are summarized in Table II. For the pure GFL inverter scheme, it lacks frequency support due to no inertia and damping. Besides, for the pure GFM inverter scheme, it has limited voltage support capability in weak grids due to poor reactive power tracking ability. However, for the mixed GFL and GFM inverter scheme, it has fast voltage and frequency support. Therefore, it is supposed that the mixed GFL and GFM scheme has more potential to meet the voltage and frequency requirements in the Grid Code. Then, an optimal proportion of mixed GFM and GFL inverters will be discussed in the next section.

Discussion of an optimal proportion of mixed GFL and GFM inverters

Considering that an optimal proportion of mixed GFL and GFM inverters depends on many factors, such as the grid strength (i.e., SCR), the required system inertia, and the amount of available energy, it might be difficult to find the absolutely optimized solution. So, only a relatively optimal solution is discussed in this paper. Assuming that there is enough energy from the energy source, then the grid strength is taken into account to analyze a relatively optimal proportion of mixed GFL and GFM inverters. As aforementioned, the capacity of the GFM inverters depends on the required active power of the power system, while the capacity of the GFL inverters depends on the required reactive power of the power system. Therefore, the proportion of GFL and GFM inverters can be determined by the required active power and reactive power of the power system, respectively.

According to the simulation results shown in Figs. 5 ~ 8, it can be seen that the weak grid case is more critical than the strong grid case in terms of the requirement of reactive power and voltage support. Hence, the proportion of the active power and reactive power can be determined by the weak grid case (e.g., SCR = 1).

Referring to [24], it is known that when the SCR is equal to 1 and the ratio of the grid impedance R_g/X_g is equal to 0.1, the maximum output active power P of the inverter is 0.9 p.u. under the condition that the apparent power S of the inverter is restricted to 1 p.u. Then, the reactive power Q can be calculated accordingly, which is 0.44 p.u. Thus, the proportion of the active power and reactive power is around 2:1. Hence, an optimal proportion of mixed GFM and GFL inverters could be 2:1. Namely, every two GFM inverters work with one GFL inverter.

Conclusion

Although the GFM inverters are deemed to be promising solutions for the future low-inertia grids, this paper reveals that a pure GFM inverter scheme may not be an optimal solution due to the limited reactive power tracking ability. Especially for the weak grid case with low SCRs, the pure GFM inverter scheme has the risk of losing voltage stability. Moreover, this paper demonstrates that a mixed GFL and GFM inverter

scheme is able to provide satisfied performance of frequency support and voltage support in either strong or weak grid cases, so that they can be implemented in renewable energy plants (e.g., wind or solar power plant). Finally, an optimal proportion of mixed GFM and GFL inverters (i.e., 2:1) is suggested for use, which can provide sufficient reactive power support in either strong or weak grid cases.

References

[1] F. Blaabjerg, Y. Yang, D. Yang, and X. Wang, "Distributed power-generation systems and protection," *Proc. IEEE*, vol. 105, no. 7, pp. 1311–1331, Jul. 2017.

[2] U. Markovic, O. Stanojev, P. Aristidou, E. Vrettos, D. Callaway, and G. Hug, "Understanding small-signal stability of low-inertia systems," *IEEE Trans. Power Syst.*, vol. 36, no. 5, pp. 3997–4017, Sep. 2021.

[3] Y. Cheng *et al.*, "Real-world subsynchronous oscillation events in power grids with high penetrations of inverter-based resources," *IEEE Trans. Power Syst.*, vol. 38, no. 1, pp. 316–330, Jan. 2023.

[4] A. Etxegarai, P. Eguia, E. Torres, A. Iturregi, and V. Valverde, "Review of grid connection requirements for generation assets in weak power grids," *Renew. Sustain. Energy Rev.*, vol. 41, pp. 1501–1514, Jan. 2015.

[5] A. Egea-Alvarez, S. Fekriasl, F. Hassan, and O. Gomis-Bellmunt, "Advanced vector control for voltage source converters connected to weak grids," *IEEE Trans. Power Syst.*, vol. 30, no. 6, pp. 3072–3081, Nov. 2015.

[6] Y. Li, L. Fan, and Z. Miao, "Stability control for wind in weak grids," *IEEE Trans. Sustain. Energy*, vol. 10, no. 4, pp. 2094–2103, Oct. 2019.

[7] Y. Khayat *et al.*, "On the secondary control architectures of ac microgrids: an overview," *IEEE Trans. Power Electron.*, vol. 35, no. 6, pp. 6482–6500, Jun. 2020.

[8] A. Pepiciello, J. L. Domínguez-García, and A. Vaccaro, "The impact of frequency support by wind turbines on the small-signal stability of power systems," *Energies*, vol. 15, no. 22, p. 8470, Nov. 2022.

[9] J. F. Morris, K. H. Ahmed, and A. Egea-Alvarez, "Analysis of controller bandwidth interactions for vector-controlled VSC connected to very weak AC grids," *IEEE J. Emerg. Sel. Top. Power Electron.*, vol. 9, no. 6, pp. 7343–7354, Dec. 2021.

[10] Y. Lamrani *et al.*, "Grid following converters stability study and control enhancements using an improved test setup," in *19th International Conference on AC and DC Power Transmission (ACDC 2023)*, Glasgow, UK, Mar. 2023, pp. 64–69.

[11] R. Rosso, X. Wang, M. Liserre, X. Lu, and S. Engelken, "Grid-forming converters: control approaches, grid-synchronization, and future trends—a review," *IEEE Open J. Ind. Appl.*, vol. 2, pp. 93–109, 2021.

[12] J. Rocabert, A. Luna, F. Blaabjerg, and P. Rodríguez, "Control of power converters in AC microgrids," *IEEE Trans. Power Electron.*, vol. 27, no. 11, pp. 4734–4749, Nov. 2012.

[13] B. Wang, Q. Lin, B. Wen, and R. Burgos, "Grid-forming distributed generation inverter control for a smooth transition from grid-connected to islanded operation mode in microgrids," in *2022 IEEE Energy Conversion Congress and Exposition (ECCE)*, Detroit, MI, USA, Oct. 2022, pp. 1–8.

[14] B. Fan and X. Wang, "Fault recovery analysis of grid-forming inverters with priority-based current limiters," *IEEE Trans. Power Syst.*, pp. 1–10, 2022, doi: 10.1109/TPWRS.2022.3221209.

[15] L. Huang, C. Wu, D. Zhou, L. Chen, D. Pagnani, and F. Blaabjerg, "Challenges and potential solutions of grid-forming converters applied to wind power generation system—an overview," *Front. Energy Res.*, vol. 11, pp. 1–14, Jan. 2023.

[16] Y. Ojo, M. Benmiloud, and I. Lestas, "Frequency and voltage control schemes for three-phase grid-forming inverters," *IFAC-Pap.*, vol. 53, no. 2, pp. 13471–13476, 2020.

[17] D. Pattabiraman, R. H. Lasseter., and T. M. Jahns, "Comparison of grid following and grid forming control for a high inverter

penetration power system," in *2018 IEEE Power & Energy Society General Meeting (PESGM)*, Portland, OR, Aug. 2018, pp. 1–5.

[18] H. Kikusato *et al.*, "Performance evaluation of grid-following and grid-forming inverters on frequency stability in low-inertia power systems by power hardware-in-the-loop testing," *Energy Rep.*, vol. 9, pp. 381–392, Mar. 2023.

[19] H. Wu and X. Wang, "Control of grid-forming VSCs: a perspective of adaptive fast/slow internal voltage source," *IEEE Trans. Power Electron.*, pp. 1–20, 2023, doi: 10.1109/TPEL.2023.3268374.

[20] L. Huang, C. Wu, D. Zhou, and F. Blaabjerg, "A double-plls-based impedance reshaping method for extending stability range of grid-following inverter under weak grid," *IEEE Trans. Power Electron.*, vol. 37, no. 4, pp. 4091–4104, Apr. 2022.

[21] L. A. M. Lima and E. H. Watanabe, "Hybrid control scheme for VSC presenting both grid-forming and grid-following capabilities," *IEEE Trans. Power Deliv.*, vol. 37, no. 6, pp. 4570–4581, Dec. 2022.

[22] L. Huang, C. Wu, D. Zhou, and F. Blaabjerg, "A power-angle-based adaptive overcurrent protection scheme for grid-forming inverter under large grid disturbances," *IEEE Trans. Ind. Electron.*, vol. 70, no. 6, pp. 5927–5936, Jun. 2023.

[23] L. Huang, C. Wu, D. Zhou, and F. Blaabjerg, "Impact of virtual admittance on small-signal stability of grid-forming inverters," in *2021 6th IEEE Workshop on the Electronic Grid (eGRID)*, New Orleans, LA, USA, Nov. 2021, pp. 1–8.

[24] L. Huang, C. Wu, D. Zhou, and F. Blaabjerg, "Grid impedance impact on the maximum power transfer capability of grid-connected inverter," in *2021 IEEE 12th Energy Conversion Congress & Exposition - Asia (ECCE-Asia)*, Singapore, Singapore, May 2021, pp. 1487–1490.